CRYSTAL GROWTH & DESIGN

Article

pubs.acs.org/crystal

Database Mining of Zeolite Structures

Peng Guo,*[,†,‡] Nana Yan,[‡,§] Lei Wang,[‡] and Xiaodong Zou*[,†]

[†]Berzelii Center EXSELENT on Porous Materials and Inorganic and Structural Chemistry, Department of Materials and Environmental Chemistry, Stockholm University, SE-106 91 Stockholm, Sweden

[‡]National Engineering Laboratory for Methanol to Olefins, Dalian National Laboratory for Clean Energy, Dalian Institute of Chemical Physics, Chinese Academy of Sciences, Dalian 116023, P. R. China

[§]University of Chinese Academy of Sciences, Beijing 100049, P. R. China

Supporting Information

ABSTRACT: Zeolites are widely used in industrial applications such as ion exchange, gas separation and adsorption, and organic catalysis. In particular, in petroleum refining and petrochemical productions, zeolites are catalysts of utmost importance. In order to classify the known zeolites and correlate the structures with their unique properties, an online Database of Zeolite Structures was established in 1996 and continuously developed by Baerlocher and McCusker at ETH-Zürich. The database contains a lot of useful structural information such as unit cell dimensions, space group, atomic coordinates of tetrahedra (T) atoms, secondary building units (SBUs), composite building units (CBUs), natural tilings, simulated powder X-ray diffraction (PXRD), etc. It has served the zeolite community for more than 20 years and has made great contributions to the development of zeolites and zeolite-related fields. In this article, we take a further step to mine the intrinsic structural information on zeolites including characteristic unit cell dimensions, butterfly layers, zeolites containing the same building layers, ABC-6 zeolite family, and recently discovered embedded isoreticular **RHO** family. The database mining of zeolite structures will shed light not only on structural correlations of related existing zeolites but also the structure determination and the further prediction of novel zeolite structures based on the existing ones, which will facilitate the target synthesis of energetically feasible hypothetical zeolite structures.

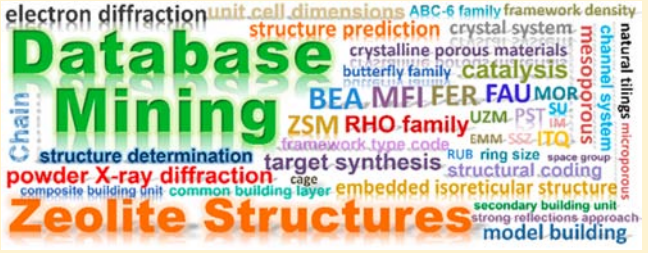

INTRODUCTION

Zeolites are crystalline microporous aluminosilicates with well-defined channels and/or cavities. The basic crystallographic building unit of a zeolite is TO_4, where the T atom can be Si or Al. Adjacent tetrahedra are connected through corner-sharing, generating a three-dimensional (3D) framework. The charge of a pure silica framework is neutral, while replacement of Si^{4+} by Al^{3+} leads to a negative charge of the entire framework. In this case, pure inorganic cations (such as Li^+, Na^+, and K^+), organic cations (such as tetramethylammonium, tetraethylammonium, and tetrapropylammonium), or their mixture are introduced into the channels or cavities, balancing the negative charge of the framework. On the basis of the number of TO_4 tetrahedra that define the pore window, zeolites can be categorized into small pore (delimited by 8 TO_4), medium pore (10 TO_4), large pore (12 TO_4), and extra-large pore (more than 12 TO_4) zeolites. Initially, the chemical compositions were restricted to Si and Al, and now they have been extended to B, P, Ti, V, Mn, Fe, Co, Ni, Zn, Ga, Ge, etc. Utilizing these chemical elements has made zeolite structures much more diverse. This extension has even opened an avenue to create ordered mesopores in zeolite structures, facilitating the mass transportation. For example, recently, Corma and our group have reported two novel mesoporous germanosilicates,[1,2] in which germanium-rich double four-ring (*d4r*) composite building units (CBUs) are frequently observed.

It is interesting to note that many zeolites have similar structural features. For example, ferrierite, ZSM-57, and ZSM-5 have a similar "butterfly" projection, in which four 5-rings connect to a 6-ring to form the wings (5-rings) and body (6-ring) of the butterfly (Figure 1). However, their 3D structures are quite different. ZSM-5 has a 3D 10 × 10 × 10-ring channel

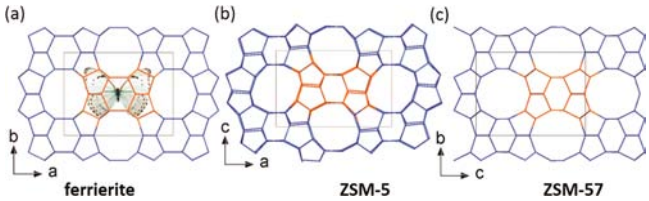

Figure 1. Structure projection of ferrierite along the *c*-axis (a), ZSM-5 along the *b*-axis (b), and ZSM-57 along the *a*-axis (c). The picture of butterfly was adopted from http://dabaoku.com/sucaidatu/dongwu/caidiehudie/web/0521029.htm.

Received: October 5, 2017
Revised: October 23, 2017
Published: November 1, 2017

DOI: 10.1021/acs.cgd.7b01410
Cryst. Growth Des. 2017, 17, 6821−6835

system, while both ZSM-57 and ferrierite possess two-dimensional (2D) 10 × 8-ring channel systems. Another example is faujasite and EMC-2, where both structures are built of the same CBUs: a sodalite (*sod*) CBU and a double 6-ring (*d6r*) CBU. In addition, the connectivities of the two CBUs are the same: each *sod* cage connects with four *d6r*s, while each *d6r* links to two *sod* cages (Figure 2a,b). However, faujasite and EMC-2 have different 3D structures and crystallize in cubic and hexagonal crystal systems, respectively (Figure 2c,d).

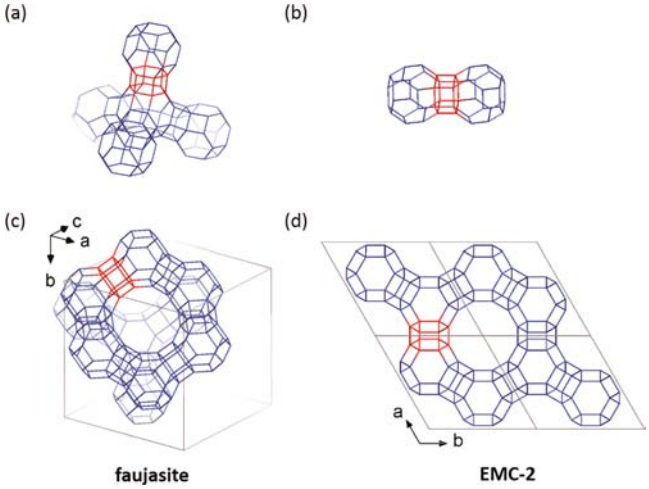

Figure 2. (a, b) The connectivity of the *sod* cage and *d6r* CBU. (c) The cubic faujasite framework. (d) The hexagonal EMC-2 framework.

The properties of a zeolite mainly depend on both the pore structures and the chemical composition. In 1970, Meier and Olson proposed the classification of zeolite materials by framework types that describe the pore structures.[3] In contrast to the zeolite framework structures that are associated with the specific compositions of zeolite materials (T = Si, Al, B, Ge, P, Co, Mg, Zn, etc.), the framework type describes the connectivity of the TO_4 tetrahedra (T = Si) in the highest symmetry, i.e., the topology of zeolites. Each framework is independent of the chemical compositions, and different zeolite structures can share the same framework type. A three-letter code has been assigned to each framework type. For example, the framework type code (FTC) of the well-known ZSM-5 structure (Zeolite Socony **M**obil-**F**ive) is **MFI**.[4] Two catalysts aluminosilicate SSZ-13 and silicoaluminophosphate SAPO-34 have different chemical compositions and share the same FTC **CHA**. An online Database of Zeolite Structures with static pages was first published in 1996 by Baerlocher at ETH-Zürich.[5] It was based on two books, *Atlas of Zeolite Structure Types* and *Collection of Simulated XRD Powder Patterns for Zeolites*, published by International Zeolite Association-Structure Commission (IZA-SC) and contained only 96 zeolite framework types.[6,7] The number of zeolite framework types in the database has now expanded to 235. Basic structural information on each framework including unit cell, space group, coordinates of the T atoms, secondary building units (SBUs), CBUs, chains, natural tiles, channel dimensionality, simulated PXRD patterns, etc. are searchable in this database.

The structural information on known zeolites described in the database can be used for structure solution of new zeolites (the details will be discussed later). Conventionally, diffraction techniques, including single crystal X-ray diffraction (SCXRD), powder X-ray diffraction (PXRD), and electron diffraction, are used for determination of zeolite structures. The amplitudes of structure factors can be exacted from diffraction data, while the phase information needed for structure solution is lost. Different algorithms and methods have been developed to deduce the structure factor phases from the diffraction data.[8−16] Zeolites often crystallize in nano- and micron-sized crystals, which are too small to be investigated by SCXRD. On the other hand, PXRD suffers from the ambiguity in the assignment of intensities caused by the overlap of reflections, structural disorder, or presence of the impurity. Recently, our research group has developed a new technique for automated collection and processing of 3D electron diffraction data of nanocrystals, called rotation electron diffraction (RED).[17,18] The diffraction data extracted from RED data can be used for *ab initio* structure determination. Various novel zeolite structures have been elucidated using RED data.[19−30] Some zeolites are not stable under electron beams so that high-quality RED data (high completeness and resolution) is difficult to collect. When the conventional diffraction methods fail, model building could be an alternative approach to determine the zeolite structures.[31−37] Thus, it is important to investigate the common structural features of known zeolites, which could be helpful for structure determination of unknown zeolites.

In this article, we present the data mining studies of the current Database of Zeolite Structures, using the basic functions of the database.[5] We have identified and summarized the similarities of the existing zeolites in this database based on crystallographic information in real space (such as characteristic unit cell dimensions and the identical building layer) and in reciprocal space (for example, the similar intensity distribution of reflections).

METHODS

In this work, the framework types rather than the framework structures are used for the investigation. Only the framework types associated with silicates, aluminosilicates, borosilicates, germanosilicates, aluminophosphates, silicoaluminophosphates, and metal aluminophosphates (metal = Co, Mg, Zn, etc.) are considered and discussed in detail. It is because the bond angles and bond lengths of frameworks associated with other type materials deviate significantly. Framework types with one unit cell dimension of approximately 5, 7.5, 8.5, and 10 Å were identified by searching unit cell less than 6 Å, between 7 and 8 Å, the narsarsukite chain, and double crankshaft chain, respectively. In the 5 Å section, the **NPO** framework will not be considered since its chemical composition is nitridophosphate. And in the 7.5 Å section, **BOF**, **SBN**, **NAB**, **LOV**, **RSN**, **VSV**, **JOZ**, **SOS**, **OSO**, and **CGF** frameworks are excluded since their of type materials are gallogermanate, beryllosilicates, zincosilicate, borogermanate, and cobalt−gallium phosphate. The inclusions of Ga, Be, Zn, B, and Co make bond angles and lengths deviate from the preset values for frameworks (T−O 1.61 Å, O−O 2.63 Å, and T−T 3.07 Å). Framework types discussed in 12.7 Å section are the extended investigation of Allen's work.[37] For the frameworks containing the butterfly layers, a search for frameworks containing the 5-1 SBU, 5-, 6-, and 10-rings or unit cell parameters around 20 and 14 Å were first conducted, and then those containing the butterfly layers were identified manually. The members of the ABC-6 family were found by searching the *a* (or *b*) value between 12.25 and 13.75 Å among the trigonal or hexagonal crystal system, while the **SOD** framework type was identified by manual checking

DOI: 10.1021/acs.cgd.7b01410
Cryst. Growth Des. 2017, 17, 6821−6835

Table 1. Twenty-Three Framework Types with a Short Axis of Approximately 5 Å

FTC	space group	a (Å)	b (Å)	c (Å)	α (deg)	β (deg)	γ (deg)	m[a]
SSY	*Pmmn*	**5.26**	22.58	13.98	90.00	90.00	90.00	yes
CAS	*Cmcm*	**5.26**	14.13	17.23	90.00	90.00	90.00	yes
JBW	*Pmma*	**5.26**	7.45	8.16	90.00	90.00	90.00	yes
MTT	*Pmmn*	**5.26**	22.03	11.38	90.00	90.00	90.00	yes
SFH	*Cmcm*	**5.25**	34.32	21.52	90.00	90.00	90.00	yes
MVY	*Pnnm*	**5.02**	8.15	13.98	90.00	90.00	90.00	no
CFI	*Imma*	13.96	**5.26**	25.97	90.00	90.00	90.00	yes
SFN	*C2/m*	25.22	**5.26**	15.02	90.00	103.89	90.00	yes
MTW	*C2/m*	25.55	**5.26**	12.12	90.00	109.31	90.00	yes
SFE	$P2_1/m$	11.46	**5.26**	13.99	90.00	100.96	90.00	yes
ABW	*Imma*	9.87	**5.25**	8.77	90.00	90.00	90.00	yes
NSI	*C2/m*	14.13	**5.25**	8.93	90.00	105.37	90.00	yes
IFO	*Pnnm*	16.44	**4.95**	22.78	90.00	90.00	90.00	no
OSI	*I4/mmm*	18.51	18.51	**5.27**	90.00	90.00	90.00	yes
ATS	*Cmcm*	13.16	21.58	**5.26**	90.00	90.00	90.00	yes
ATN	*I4/mmm*	13.07	13.07	**5.26**	90.00	90.00	90.00	yes
BIK	*Cmcm*	7.54	16.22	**5.26**	90.00	90.00	90.00	yes
TON	*Cmcm*	14.11	17.84	**5.26**	90.00	90.00	90.00	yes
BCT	*I4/mmm*	8.95	8.95	**5.26**	90.00	90.00	90.00	yes
GON	*Cmmm*	16.90	20.40	**5.26**	90.00	90.00	90.00	yes
CAN	$P6_3/mmc$	12.49	12.49	**5.25**	90.00	90.00	120.00	yes
ATO	$R\bar{3}m$	20.91	20.91	**5.06**	90.00	90.00	120.00	no
VET	$P\bar{4}$	13.05	13.05	**4.95**	90.00	90.00	90.00	no

[a]The mirror planes are normal to the single or double zigzag chains.

each framework due to its cubic unit cell settings. Zeolite frameworks built by the same layers were identified by carefully checking each framework in the database. The members in the **RHO** family (including **RHO**, **PAU**, and **MWF** in the database) were found by identifying the similar distribution of strong reflections in reciprocal space.[29]

RESULTS AND DISCUSSION

Characteristic Structural Information Hinted by the Unit Cell Dimensions. *5 Å.* Table 1 lists the 23 framework types with one unit cell dimension of ca. 5 Å (4.95−5.27 Å). This value is the typical periodicity of a double or single zigzag chain, as seen in the **CAN** (Figure 3a,b) and **MVY** (Figure 3d,e) framework types. It is also worth noting that both frameworks have one-dimensional (1D) channels along this 5 Å axis, as shown in Figure 3b,e. According to the space group $P6_3/mmc$ of **CAN**, there is a mirror plane perpendicular to the 5 Å axis. Consequently, all T atoms in the **CAN** framework have to be located on the mirror plane to avoid too short interatomic distances due to the short *c*-axis (special positions, Figure 3c). For the **MVY** framework with the space group *Pnnm*, there is an *n* glide plane rather than a mirror plane perpendicular to the 5 Å axis. The glide plane does not generate too short interatomic distances. Therefore, T atoms do not need to be at the glide plane and can be located at general positions (Figure 3f).

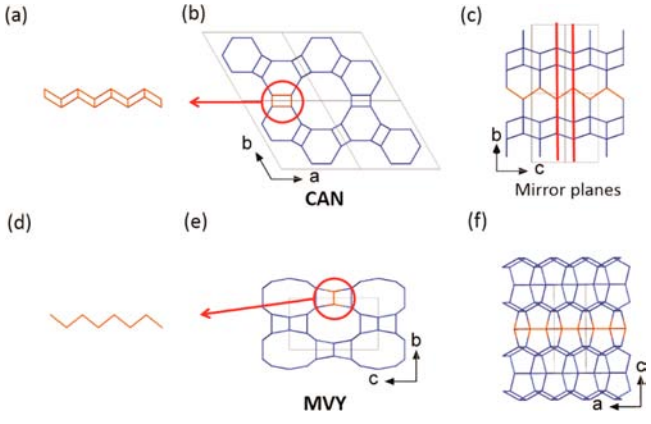

Figure 3. (a) The double zigzag chain. (b, c) The **CAN** framework type viewed along [001] and [100], respectively. (d) The single zigzag chain. (e, f) The **MVY** framework type viewed along [100] and [010], respectively. Both double and single zigzag chains are highlighted in orange. The 5 Å axis is the *c*-axis in **CAN** and *a*-axis in **MVY**.

Three general rules are drawn for the 23 framework types with ca. 5 Å unit cell dimension:

(1) The framework has a 1D channel along the 5 Å axis.
(2) If there is a mirror plane perpendicular to the 5 Å axis, all the T atoms must be located on the mirror plane.
(3) All the frameworks are built by the single or double zigzag chains. It is possible to distinguish single and double zigzag chains by IR or Raman spectroscopy; the double zigzag chain is composed of 4-rings, which can be identified from their characteristic IR peaks (500−650 cm^{-1}) and Raman peaks (480−520 cm^{-1}) spectra.[38]

7.5 Å. Among the 235 framework types, at least 33 have one unit cell dimension of ca. 7.5 Å (7.00−7.81 Å), as listed in Table 2. The structural features of this group are much more interesting and complex than those with 5 Å axis. Six types of chains are found in this group; one of them is associated with a single saw chain, while the other five are done with a double saw chain, as shown in Scheme 1a. A typical double saw chain contains three edge-sharing 4-rings and has a periodicity of ca. 7.5 Å (Scheme 1a and Figure 4a), denoted "Type A, 4-4-4-double saw chains" here. It can be found in the **MOZ**, **EON**, **ATT**, **OWE**, **MAZ**, **LTF**, **LTL**, **OFF**, and **-WEN** framework

DOI: 10.1021/acs.cgd.7b01410
Cryst. Growth Des. 2017, 17, 6821−6835

Table 2. Thirty-Three Framework Types with One Axis of Approximately 7.5 Å

FTC	space group	a (Å)	b (Å)	c (Å)	α (deg)	β (deg)	γ (deg)	m[a]	m or g[b]	8-rings[c]	types of chain
RWR	$I4_1/amd$	**7.81**	**7.81**	27.35	90.00	90.00	90.00	yes	yes	yes	C
EON	$Pmmn$	**7.57**	18.15	25.93	90.00	90.00	90.00	yes	yes	yes	A
CDO	$Cmcm$	**7.56**	18.72	14.10	90.00	90.00	90.00	yes	yes	yes	C
ETL	$Cmcm$	**7.55**	29.16	18.13	90.00	90.00	90.00	yes	yes	yes	C/D
MFS	$Imm2$	**7.54**	14.39	19.02	90.00	90.00	90.00	yes	yes	yes	C/D
BIK	$Cmcm$	**7.54**	16.22	5.26	90.00	90.00	90.00	yes	yes	yes	B
RRO	$P2/c$	**7.41**	8.64	17.18	90.00	113.68	90.00	no	yes	yes	F
MON	$I4_1/amd$	**7.14**	**7.14**	17.81	90.00	90.00	90.00	yes	yes	yes	B
DFT	$P4_2/mmc$	**7.07**	**7.07**	9.02	90.00	90.00	90.00	yes	yes	yes	B
UOS	$Pmma$	19.91	**7.55**	9.07	90.00	90.00	90.00	yes	yes	yes	D
DAC[d]	$C2/m$	18.57	**7.54**	10.38	90.00	108.92	90.00	yes	no	yes	C
ATT	$Pmma$	9.98	**7.54**	9.37	90.00	90.00	90.00	yes	yes	yes	A
JBW	$Pmma$	5.26	**7.45**	8.16	90.00	90.00	90.00	yes	yes	yes	B
OWE	$Pmma$	14.36	**7.17**	9.08	90.00	90.00	90.00	yes	yes	yes	B/A
THO	$Pmma$	14.00	**7.00**	6.48	90.00	90.00	90.00	yes	yes	yes	B
IFR	$C2/m$	18.63	13.44	**7.63**	90.00	102.32	90.00	no	yes	no	E
AWW	$P4/nmm$	13.63	13.63	**7.63**	90.00	90.00	90.00	no	yes	no	E
MAZ	$P6_3/mmc$	18.10	18.10	**7.62**	90.00	90.00	120.00	yes	yes	yes	A
LAU	$C2/m$	14.59	12.88	**7.61**	90.00	111.16	90.00	no	yes	no	E
BRE	$P2_1/m$	6.76	17.09	**7.60**	90.00	95.83	90.00	no	yes	yes	F
LTF	$P6_3/mmc$	31.17	31.17	**7.60**	90.00	90.00	120.00	yes	yes	yes	A
LTL	$P6/mmm$	18.13	18.13	**7.57**	90.00	90.00	120.00	yes	yes	yes	A
OFF	$P\bar{6}m2$	13.06	13.06	**7.57**	90.00	90.00	120.00	yes	yes	yes	A
-WEN	$P\bar{6}2m$	13.59	13.59	**7.56**	90.00	90.00	120.00	yes	yes	-[e]	A
MOZ	$P6/mmm$	31.20	31.20	**7.55**	90.00	90.00	120.00	yes	yes	yes	A
MOR	$Cmcm$	18.26	20.53	**7.54**	90.00	90.00	90.00	yes	yes	yes	C
FER	$Immm$	19.02	14.30	**7.54**	90.00	90.00	90.00	yes	yes	yes	C
SZR	$Cmmm$	18.87	14.40	**7.51**	90.00	90.00	90.00	yes	yes	yes	D
STF	$C2/m$	14.10	18.21	**7.48**	90.00	98.99	90.00	no	yes	no	E
RTE	$C2/m$	14.10	13.67	**7.43**	90.00	102.42	90.00	no	yes	no	E
HEU	$C2/m$	17.52	17.64	**7.40**	90.00	116.10	90.00	no	yes	yes	F
MTF	$C2/m$	9.63	30.39	**7.25**	90.00	90.45	90.00	no	yes	no	E
SFF	$P2_1/m$	11.45	21.70	**7.23**	90.00	93.15	90.00	no	yes	no	E

[a]The mirror planes are normal to type A, B, C, D, E, and F. [b]The mirror planes or glide planes are normal to the other two axes, rather than the 7.5 Å axis which is along the characteristic chain. [c]The 8-ring pore openings are in the crystallographic plane containing this unique axis. [d]The 8-ring pore openings in the DAC framework type in the *ab*-plane are generated by the type B chain through the (0.5, 0.5, 0) translation, rather than the mirror or the glide plane. [e]The 10-ring pore opening in the -**WEN** framework type is observed along the <100> direction.

types. The other five types of chains are the single saw chain, 8-, 5-4-5, 4-6, and 4-4-5-double saw chains, denoted Type B, C, D, E, and F, respectively (Scheme 1a and Figure 4b–f).

By investigating the structural features of the 33 framework types in this section, the following two general rules can be applied to most of the framework types as illustrated in Scheme 1:

(1) These six types of chains could be categorized into two groups by identifying the mirror symmetry normal to the chains (7.5 Å axis). For instance, if there is a mirror plane normal to the 7.5 Å axis, the framework should contain the chains of Type A/B/C/D. In contrast, an absence of the mirror plane perpendicular to the 7.5 Å axis indicates that the frameworks are composed of the chains of Type E/F. It also implies the former four types of chains are symmetric, while the latter two types are asymmetric, as seen in Scheme 1b.

(2) Except for the Type E-chain, all the other five chains of Types A/B/C/D/F can form 8-ring pores with a neighboring chain related by a mirror plane or glide plane in parallel to the 7.5 Å axis (another description is that there is a mirror plane or glide plane normal to the other axes), as illustrated in Scheme 1c.

The frameworks containing the Type A-chain follow both rules. The **MOZ** framework type is selected as an example. It contains the Type A chain, running along the *c*-axis (ca. 7.55 Å) (Figure 4g). Its space group is *P6/mmm*, with a mirror plane normal to the *c*-axis. Therefore, it follows the first rule. The mirror planes perpendicular to the *a*- and *b*-axis are also present based on its space group. It indicates the 8-ring pore openings can be found in the *ac*- or *bc*-plane (Figure 4m), following the second rule. The periodicity of Type A is in the range between 7.54 and 7.62 Å. In addition, most frameworks in this category have hexagonal structures.

In order to further illustrate the aforementioned two rules, frameworks with single saw chains are also chosen as samples. The single saw chain (Type B-chain) emerges in the **MON** framework along its *a* (or *b*)-axis (Figure 4h). For clarity, the following description adopts Type B-chain along the *a*-axis as shown in Figure 4b. Its space group $I4_1/amd$ suggests there are mirror planes normal to the *a*-axis (7.14 Å), corresponding to the symmetric Type B-chain. And the mirror plane normal to *b*-axis generates 8-ring pore openings in the *ab*-plane in this

DOI: 10.1021/acs.cgd.7b01410
Cryst. Growth Des. 2017, 17, 6821–6835

Scheme 1. (a) The Six Types of Chains Found in Zeolites Frameworks That Have a Periodicity of ca. 7.5 Å. (b) The Six Chain Types Are Divided into Two Groups According to Whether There Is a Mirror Symmetry Perpendicular to the Chain (7.5 Å axis). (c) Two Chains Related by a Mirror or Glide Plane Parallel to the Chains That Generate Possible Eight-Ring Pores except for the Type E-Chain

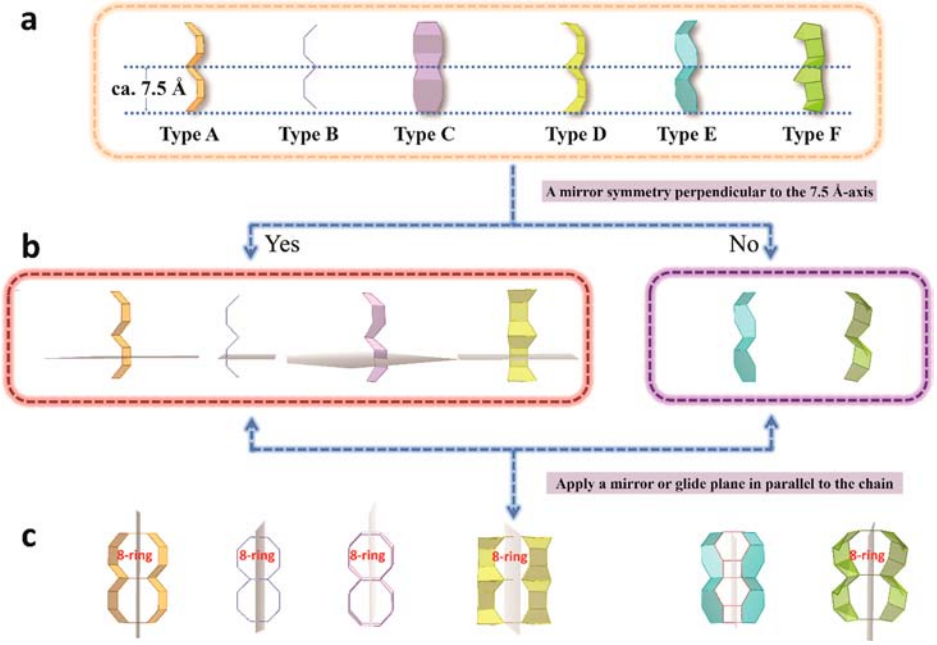

framework (Figure 4n). Framework types such as **BIK**, **DFT**, **JBW**, **OWE**, and **THO** also have the Type B-chain, and the 8-ring pore openings could be observed.

The 8-double saw chain (Type C-chain) is made up of undulating 8-rings (Figure 4c). It can be considered as part of the *mor* CBU chain (Figure 4c). In this case, the 8-ring pore opening within the Type C-chain is blocked by the extra T atoms, which are highlighted in red. Choose the **FER** framework type as an example. Since the *mor* CBU chains are observed along the *c*-axis (7.54 Å) (Figure 4i), the **FER** framework type has the Type C-chain (Figure 4c). Its space group *Immm* indicates there is a mirror plane perpendicular to the *c*-axis, which follows the first rule. There are also mirror planes normal to the *a*- and *b*-axis, and therefore, the 8-ring pore openings are expected to appear in the *ac* or *bc*-plane. After this framework was carefully checked, 8-ring openings are present in the *ac*-plane (Figure 4o), following the second rule. Other framework types as **RWR**, **CDO**, **ETL**, **MFS**, **DAC**, and **MOR** also belong to this category.

The Type D-chain contains one 4-ring and two 5-rings within one periodicity (Figure 4d). Only four frameworks (**UOS**, **ETL**, **MFS**, and **SZR**) belong to this category. Two of them (**ETL** and **MFS**) have the Type C-chain as well, which were mentioned in the last paragraph. Considering the framework type **UOS** as an example, this characteristic chain runs along its *b*-axis (Figure 4j), and there is a mirror plane perpendicular to it according to its space group (*Pmma*). An *a* glide plane perpendicular to the *c*-axis generates 8-ring pore openings in the *bc*-plane (Figure 4p).

Compared with the symmetrical type A/B/C/D, the chains of type E/F are asymmetric due to the lack of the mirror planes normal to the chain (Figure 4e,f). For the frameworks containing Type E, although mirror planes or glide planes applying to the other two main axes are present, no 8-ring pore opening is observed (Scheme 1c, Type E). For example, in the **STF** framework type, the Type E-chain along the *c*-axis is identified (Figure 4k). According to its space group (*C*2/*m*), there is no mirror plane normal to this unique axis, whereas the mirror plane perpendicular to its *b*-axis is found. However, no pore opening is generated in the *ac*- or *bc*-plane (Figure 4q), thus leaving the 1D channel system along the *c*-axis. The frameworks such as **IFR**, **AWW**, **LAU**, **RTE**, **MTF**, and **SFF** have the identical structural feature.

Three framework types **RRO**, **BRE**, and **HEU** contain the Type F 4-4-5-double saw chain, which lacks the mirror symmetry perpendicular to the chain. The Type F-chain can be regarded as a part of the *bre* CBU chain (Figure 4f). Unlike frameworks with the Type E-chain, a mirror plane or glide plane in parallel to the chain can still generate 8-ring pore openings. For instance, the framework type **RRO** contains the type F-chain along the *a*-axis (7.41 Å) (Figure 4l). The *c* glide plane normal to the *b*-axis (deduced from its space group *P*2/*c*) generates 8-ring pore openings in the *ab*-plane (Figure 4r). Framework types **BRE** and **HEU** also contain the Type F-chain.

8.5 Å. The chains with ca. 5 and 7.5 Å described in the previous sections consist of two and three T atoms in the repeating unit, respectively. When four T atoms are included in the repeating unit, the unit cell dimension can range from 8 to 10 Å, and the structural diversity is also enhanced. In order to simplify the classification, we mainly investigated those containing narsarsukite chains (denoted *nsc*) and their derivatives with the periodicity of ca. 8.5 Å (8.26−9.02 Å), and double crankshaft chains (designated *dcc*) with the periodicity of ca. 10 Å (to be discussed in the next section), respectively.

The unique single narsarsukite chain was originally found in the natural mineral narsarsukite ($Na_4Ti_2Si_8O_{22}$). It can be described as twisted single 4-rings linked in a face-to-face mode (Figure 5a). The single narsarsukite chain (*nsc*, denoted Type

DOI: 10.1021/acs.cgd.7b01410
Cryst. Growth Des. 2017, 17, 6821−6835

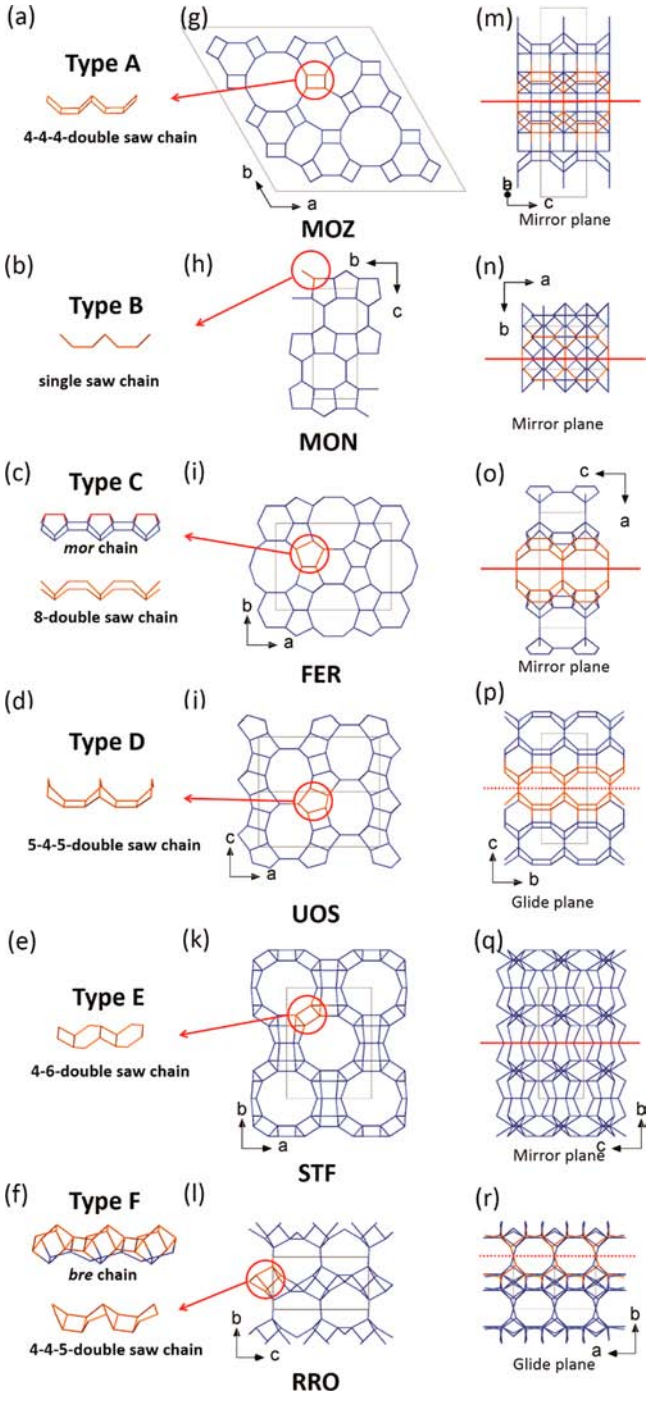

Figure 4. (a–f) The six single or double saw chains found in zeolite frameworks. (a) Type A 4-4-4-double saw chain, (b) Type B single saw chain, (c) Type C 8-double saw chain, (d) Type D 5-4-5-double saw chain, (e) Type E 4-6-double saw chain, and (f) Type F 4-4-5-double saw chain. (g–r) The framework type of **MOZ** (g, m), **MOZ** (h, n), **FER** (i, o), **UOS** (j, p), **STF** (k, q), and **RRO** (l, r). The characteristic chains and 8-ring pore openings are highlighted in orange. The *mor* chain in (c) can be described as the 8-double saw chain (in blue) connected by extra T atoms (in red). (f) Type F 4-4-5-double saw chain is part of the *bre* chain highlighted in orange.

A) can be found in nine framework types: **APD**, **ATV**, **AEL**, **PSI**, **DFT**, **AFI**, **AET**, **AFO**, and **SAF** (as listed in Table 3). Figure 5d,g shows the **AFO** framework viewed along and perpendicular to the *nsc*, respectively.

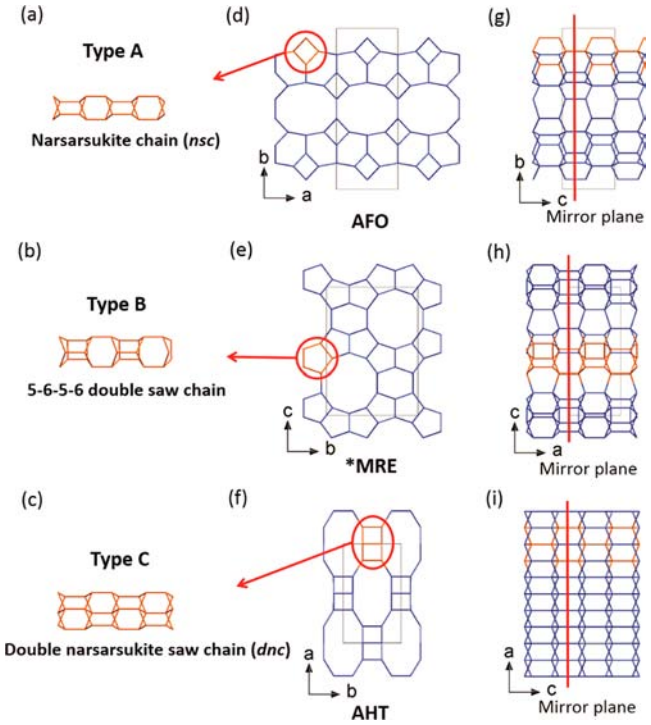

Figure 5. (a) The narsarsukite chain. (d, g) The **AFO** framework type viewed along the [001] and [100] directions, respectively. (b) The 5-6-5-6-double saw chain. (e, h) The ***MRE** framework type viewed along the [100] and [010] directions, respectively. (c) The double narsarsukite chain. (f, i) The **AHT** framework type viewed along the [001] and [010] directions, respectively.

If the twisted single 4-rings in the narsarsukite chain are replaced by single 5-rings, a new 5-6-5-6 double saw chain (denoted Type B) is formed, as shown in Figure 5b. The chain has a similar periodicity as the narsarsukite chain. Three framework types ***MRE**, ***STO**, and **DON** contain the 5-6-5-6 double saw chain. Figure 5, panels e and h show the ***MRE** framework viewed along and perpendicular to this chain, respectively.

Three framework types **AET**, **AHT**, and **VFI** have the double narsarsukite chain (*dnc*, denoted Type C, shown in Figure 5c), which is also regarded as another derivative of the typical single narsarsukite chain. For instance, the **AHT** framework is shown in Figure 5, panels f and i, viewed along and perpendicular to the *dnc*, respectively.

The following two common features are found among the framework types containing an 8.5 Å axis:

(1) There is a mirror plane perpendicular to the 8.5 Å axis.
(2) The framework contains always channels along the 8.5 Å axis, and seldom channels perpendicular to the 8.5 Å axis. Among the 14 framework types, only **APD** and **DFT** have distorted (elliptical) 8-ring channels with small pore openings (the shortest diameter <2.4 Å) perpendicular to the 8.5 Å axis.

Double Crankshaft Chain (10 Å). Ten framework types containing the double crankshaft chain (*dcc*, Figure 6a) were identified as listed in Table 4. The periodicity of the *dcc* in these frameworks ranges from 8.39 to 9.98 Å. Except for ***STO** and **DON**, the two general rules used in 7.5 Å section can also be applied here. For example, the double crankshaft chain is identified along the *c*-axis in the **MER** framework (Figure 6b). The symmetric double crankshaft chain implies that there

DOI: 10.1021/acs.cgd.7b01410
Cryst. Growth Des. 2017, 17, 6821–6835

Table 3. Fourteen Framework Types with One Axis of Approximately 8.4 Å

FTC	space group	*a* (Å)	*b* (Å)	*c* (Å)	*α* (deg)	*β* (deg)	*γ* (deg)	*m*[a]	8-rings[b]	types of chain
APD	*Cmce*	**8.72**	20.06	10.17	90.00	90.00	90.00	yes	yes	A
ATV	*Cmme*	**8.58**	15.31	9.66	90.00	90.00	90.00	yes	no	A
AEL	*Imma*	**8.31**	18.73	13.39	90.00	90.00	90.00	yes	no	A
PSI	*Cmce*	**8.26**	22.35	37.76	90.00	90.00	90.00	yes	no	A
***MRE**	*Imma*	**8.26**	14.56	20.31	90.00	90.00	90.00	yes	no	B
***STO**	*P*12/*m*1	29.89	**8.39**	24.73	90.00	105.05	90.00	yes	no	B
DFT	$P4_2/mmc$	7.08	7.08	**9.02**	90.00	90.00	90.00	yes	yes	A
AHT	*Cmcm*	15.79	9.21	**8.59**	90.00	90.00	90.00	yes	no	C
VFI	$P6_3/mcm$	18.28	18.28	**8.59**	90.00	90.00	120.00	yes	no	C
AFI	*P*6/*mcc*	13.83	13.83	**8.58**	90.00	90.00	120.00	yes	no	A
DON	*Cmcm*	18.89	23.37	**8.47**	90.00	90.00	90.00	yes	no	B
AET	*Cmcm*	32.83	14.38	**8.35**	90.00	90.00	90.00	yes	no	A/C
AFO	*Cmcm*	9.76	25.61	**8.33**	90.00	90.00	90.00	yes	no	A
SAF	*Ibam*	14.71	27.54	**8.32**	90.00	90.00	90.00	yes	no	A

[a]The mirror planes are normal to the Type A, B, and C. [b]The 8-ring pore openings are in the crystallographic plane containing this unique axis.

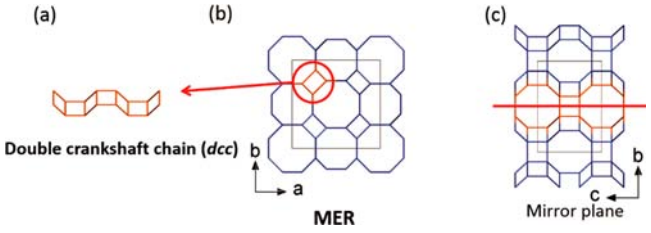

Figure 6. (a) Double crankshaft chain. (b–c) The **MER** framework type viewed along the chain ([001]) and perpendicular to the chain ([100]).

should be mirror planes normal to it, which is confirmed by the symmetry operations deduced from its space group (*I*4/*mmm*). Mirror planes normal to the *a*- and *b*-axis are also present based on the symmetry operations. According to the second rule described in the 7.5 Å section, 8-ring pore openings in the *ac*- or *bc*-plane will be generated (Figure 6c). Both rules can be applied to the **APC**, **ATT**, **AWO**, **PHI**, **SIV**, **GIS**, and **GME** frameworks.

The frameworks ***STO** and **DON** contain two types of chains: *nsc* and *dcc* along the same axis. The periodicity is determined by that of the *nsc* in the ***STO** and **DON** frameworks, and therefore the periodicity of their *dcc* is smaller (8.39 and 8.47 Å, respectively) than the others. The double crankshaft chains in ***STO** and **DON** are responsible for connecting with 2D layers or 1D column (Figure S1), respectively.

12.7 Å. In 2007, Burton et al. reported a new zeolite SSZ-65 (**SSF**) possessing 2D intersecting 12-ring channels with pore apertures of 6.9 Å × 5.9 Å.[39] The framework is built by columns constructed of alternating *d*6*rs* or 6^24^6 (6^24^6 represents a CBU containing two 6-rings and six 4-rings) and a pair of 6^8 CBUs (*mso*), as shown in Figure 7. The periodicity of this column corresponds to the *c*-parameter (12.79 Å). The authors made further efforts to summarize a series of zeolite

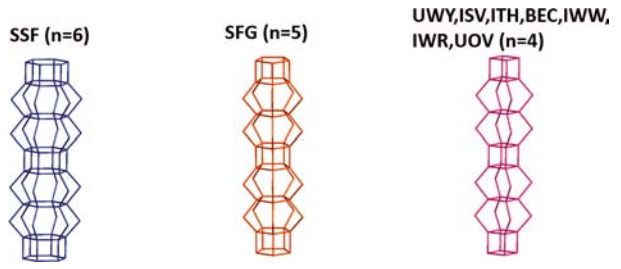

Figure 7. Repeating unit (12.7 Å) in the framework types of **SSF**, **SFG**, **UWY**, **ISV**, **ITH**, **BEC**, **IWW**, **IWR**, and **UOV**.

Table 4. Ten Framework Types with One Axis of Approximately 10 Å

FTC	space group	*a* (Å)	*b* (Å)	*c* (Å)	*α* (deg)	*β* (deg)	*γ* (deg)	*m*[a]	*m* or *g*[b]	8-rings[c]
ATT	*Pmma*	**9.98**	7.51	9.37	90.00	90.00	90.00	yes	yes	yes
PHI	*Cmcm*	**9.89**	14.06	14.05	90.00	90.00	90.00	yes	yes	yes
SIV	*Cmcm*	**9.88**	14.08	28.13	90.00	90.00	90.00	yes	yes	yes
GIS	$I4_1/amd$	**9.80**	9.80	10.16	90.00	90.00	90.00	yes	yes	yes
AWO	*Cmce*	**9.10**	15.04	19.24	90.00	90.00	90.00	yes	yes	yes
APC	*Cmce*	**8.99**	19.36	10.39	90.00	90.00	90.00	yes	yes	yes
***STO**[d]	*P*2/*m*	29.89	**8.39**	24.73	90.00	105.05	90.00	yes	no	no
MER	*I*4/*mmm*	14.01	14.01	**9.95**	90.00	90.00	90.00	yes	yes	yes
GME	$P6_3/mmc$	13.67	13.67	**9.85**	90.00	90.00	120.00	yes	yes	yes
DON[d]	*Cmcm*	18.89	23.37	**8.47**	90.00	90.00	90.00	yes	yes	no

[a]The mirror planes are normal to the double crankshaft chains. [b]The mirror planes or glide planes are normal to the other two axes, rather than the 10 Å axis. Another description is that the mirror planes or glide planes are parallel to this unique axis. [c]The 8-ring pore openings are in the crystallographic plane containing this 10 Å axis. [d]***STO** and **DON** frameworks contain both double crankshaft and narsarsukite chains along the same axis. The shorter periodicity along this unique axis in both frameworks is determined by the narsarsukite chains, rather than double crankshaft chains.

DOI: 10.1021/acs.cgd.7b01410
Cryst. Growth Des. 2017, 17, 6821–6835

Table 5. Nine Framework Types with One Axis around 12.7 Å

FTC	space group	a (Å)	b (Å)	c (Å)	α (deg)	β (deg)	γ (deg)
ISV	$P4_2/mmc$	**12.87**	**12.87**	25.67	90.00	90.00	90.00
BEC	$P4_2/mmc$	**12.77**	**12.77**	12.98	90.00	90.00	90.00
UOV	$Amm2$	**12.72**	21.99	38.76	90.00	90.00	90.00
ITH	$Amm2$	**12.57**	11.66	21.93	90.00	90.00	90.00
UWY	$Pmmm$	25.11	**12.73**	11.51	90.00	90.00	90.00
IWW	$Pbam$	41.69	**12.71**	**12.71**	90.00	90.00	90.00
SFG	$Pmma$	25.53	**12.57**	13.07	90.00	90.00	90.00
SSF	$P6/mmm$	17.21	17.21	**12.80**	90.00	90.00	120.00
IWR	$Cmmm$	21.23	13.30	**12.68**	90.00	90.00	90.00

frameworks with the similar structural features. They proposed that other six framework types contain two consecutive n^26^n cages followed by an n^24^n cage along the 12.7 Å-axis (where n = 6 for **SSF**, n = 5 for **SFG**, and n = 4 for **ISV**, **ITH**, **BEC**, **IWW**, and **IWR**). After that work, Dodin et al. reported in 2010 a new framework **UWY** with the b-parameter of ca. 12.7 Å.[40] And Lorgouilloux et al. reported in 2014 another new framework **UOV** with the a-parameter of ca. 12.7 Å.[28] Both structures have the structural columns constructed of alternating 4^4 ($d4r$) CBU and dual 4^26^4 (lau) CBUs along this unique axis. Thus, there are nine frameworks in all (listed in Table 5) as shown in Figure 7.

Butterfly Layer. As mentioned in the introduction, ferrierite (FTC: **FER**), ZSM-57 (**MFS**), and ZSM-5 (**MFI**) have the similar butterfly layer. There are other seven framework types built by this butterfly layer solely (as seen in Figure 8).[41] In order to compare these 10 framework types conveniently and efficiently, their unit cell settings are reconfigurated as listed in Table 6. The 2D unit cell dimensions of the butterfly layer are a ≈ 14 Å, b ≈ 20 Å, and γ = 90°. Each node in the layer has three connections, leaving the fourth one pointing up or down. The connectivity of adjacent nets is via mirror planes or inversion centers. It is worth noting that the channel running direction can be deduced from the small deviations of the 2D unit cell dimensions. Since the butterfly layer in the ***MRE** framework type is relative flat, the stacking of this layer along the c-axis is close, only creating a 10-ring channel perpendicular to this layer. In this case, its 2D unit cell dimensions (a = 14.56 Å, b = 20.31 Å, and γ = 90°) are used as a reference. The a-parameter of the **BOG** framework is 1.89 Å shorter than that of the ***MRE** framework. This means the butterfly layer in the **BOG** framework is no longer flat, but corrugating along the a-axis, thus creating channels running along the b-axis (as shown in Figure 8, **BOG**). This analysis can also be applied to **MFI** and **MEL** framework types (as illustrated in Figure 8, **MFI** and **MEL**). For **IMF**, **FER**, **MFS**, and **SZR** framework types, their b-parameters are shorter than the one of the ***MRE** framework, so that channels running along the a-axis can be observed (see Figure 8 **IMF**, **FER**, **MFS**, and **SZR**). A comparison of the 2D unit cell dimensions of the butterfly layer shows that there is a direct relation between the shortened dimension and the existence of channels. This means if there is a shorter axis compared with the corresponding one of ***MRE**, channels running along the other axis will be observed. This rule can even be applied to the analysis of channel system in the complex **TUN** framework. Compared with ***MRE**, both the a- and b-parameters of **TUN** shrink, by 0.64 and 0.71 Å, respectively. Consequently, channels running the diagonal of the 2D unit cell are generated, as seen in Figure 8 **TUN**. Although the b-axis of the **TON** framework is 2.47 Å shorter than that of ***MRE**, which is the largest deviation among the members of the butterfly family, no pore openings along the a-axis are observed. It is mainly because **TON** has a very short unit cell (5.26 Å) along the c-axis, precluding the presence of any channels along the a- or b-axis.

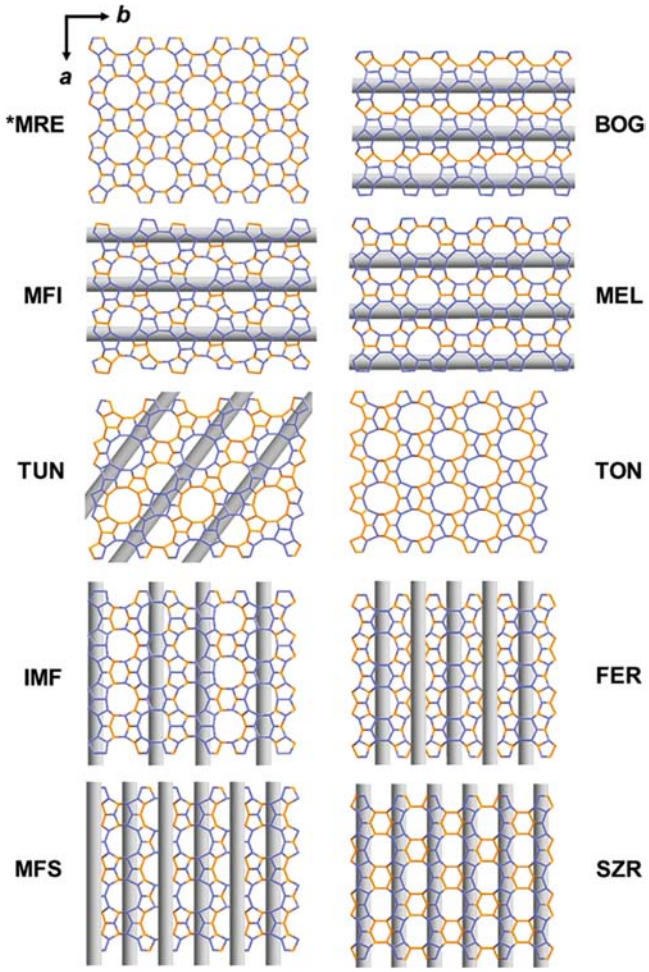

Figure 8. Butterfly layers extracted from the 10 members of the butterfly family viewed perpendicular to the layer. The light gray stripes indicate the channels formed as a result of the corrugation of the layer. Only the T−T connections (T = Si, Al) are shown for clarity. The T atoms pointing up are in blue, and those pointing down are in gold. Reprinted with permission from ref 39. Copyright 2015, Walter de Gruyter GmbH.

Zeolite Structures Constructed from the Same Building Layers. In the preceding section, we have introduced a specific butterfly layer and found that the deviations of the 2D unit cell of the butterfly layer can provide hints about the running

DOI: 10.1021/acs.cgd.7b01410
Cryst. Growth Des. 2017, 17, 6821−6835

Table 6. Unit Cell Parameters (a, b, and c) with Reconfigured Unit Cell Settings, Space Groups, and Channel Dimension for the Ten Members of the Butterfly Family of Zeolites

FTC	a (Å)	b (Å)	c (Å)	Δa (Å)[a]	Δb (Å)[a]	space group[b]	channel dimension
*MRE	14.56	20.31	8.26			*Imcm*	1D
BOG	12.67	20.01	23.58	1.89	0.30	*Ibmm*	3D
MFI	13.14	20.09	19.74	1.42	0.22	*Pbnm*	3D
MEL	13.46	20.27	20.27	1.10	0.04	$I\bar{4}m2$[c]	3D
TUN	**27.85**	19.60	20.02	0.64[d]	0.71	$B112/m$[e]	3D
TON	14.11	17.84	5.26	0.45	2.47	*Cmcm*	1D
IMF	14.30	**56.79**	20.29	0.26	1.38[g]	*Cmcm*	3D
FER	14.30	19.02	7.54	0.26	1.29	*Immm*	2D
MFS	14.39	19.02	7.54	0.17	1.29	*Im2m*	2D
SZR	14.40	18.87	7.514	0.16	1.44	*Cmmm*	3D

[a] Δa and Δb are the differences between a and b parameters and those of *MRE. [b] The space groups have been changed to reflect the new unit cell settings, with the exception of the tetragonal unit cell used for MEL. [c] The original space group is given here. The −4 symmetry operation is along the a-axis in the new unit cell. [d] This value has been calculated using $a/2$. [e] The unique axis is the c-axis and $\gamma = 93.2°$. The full H-M symbol is given here for clarity. [f] The 10-ring channels are along the $[1\bar{1}0]$ direction. [g] This value has been calculated using $b/3$.

Table 7. Ten Groups of 3D Zeolite Frameworks Containing the Same Building Layers

	FTC	space group	a (Å)	b (Å)	c (Å)	α (deg)	β (deg)	γ (deg)
I	FER	*Immm*	19.02	14.30	7.54	90.00	90.00	90.00
	CDO	*Cmcm*	7.56	18.72	14.10	90.00	90.00	90.00
II	MFI	*Pnma*	20.09	19.74	13.14	90.00	90.00	90.00
	MEL	$I\bar{4}m2$	20.27	20.27	13.46	90.00	90.00	90.00
III	NSI	$C2/m$	14.13	5.25	8.93	90.00	90.00	90.00
	CAS	*Cmcm*	5.26	14.13	17.23	90.00	90.00	90.00
IV	HEU	$C2/m$	17.52	17.64	7.40	90.00	116.10	90.00
	RRO	$P2/c$	7.41	8.64	17.18	90.00	113.68	90.00
V	FAU	$Fd\bar{3}m$	24.06	24.06	24.06	90.00	90.00	90.00
	EMT	$P6_3/mmc$	17.22	17.22	28.08	90.00	90.00	120.00
VI	SFO	$C2/m$	22.59	13.57	6.97	90.00	99.02	90.00
	AFR	*Pmmn*	22.31	13.57	6.97	90.00	90.00	90.00
VII	IWW	*Pbam*	41.69	12.71	12.71	90.00	90.00	90.00
	ITG	$P2/m$	12.74	12.70	21.00	90.00	96.29	90.00
VIII	ITH	*Amm2*	12.57	11.66	21.93	90.00	90.00	90.00
	ITR	*Cmcm*	11.67	22.00	25.17	90.00	90.00	90.00
IX	ITE	*Cmcm*	20.75	9.80	20.01	90.00	90.00	90.00
	RTH	$C2/m$	9.76	20.53	10.00	90.00	96.90	90.00
X	ZON	*Pbcm*	6.92	14.87	17.24	90.00	90.00	90.00
	JSN	$P2/c$	8.72	6.92	14.95	90.00	96.99	90.00

directions of channels. In this section, 10 zeolite groups, in which two members share the same zeolitic layer, were identified as listed in Table 7. For example, both the **FER** and **CDO** frameworks have a similar orthorhombic unit cell and are built of edge-sharing *fer* CBUs. Figure 9a,b shows the *fer* CBU in the **FER** framework viewed along different directions. Each *fer* CBU connects with four adjacent ones to generate a 2D structure as illustrated in Figure 9c,d. Two neighbor layers are linked through the mirror plane, forming the 3D **FER** framework as shown in Figure 9e. If the upper layer highlighted in Figure 9e is translated by $1/2b$ relative to the bottom one, the framework **CDO** is generated, as demonstrated in Figure 9f. Alternating 6- and 10-ring channels are present between the layers in the **FER** framework, while only 8-ring channels are observed between the layers in the **CDO** framework.

In some cases, being familiar with unit cell dimensions of the 2D zeolitic layers will be helpful for the structure determination of new zeolites by model building. For example, the structure of ITQ-38 was solved by Willhammar et al. at Stockholm University, who derived its monoclinic unit cell from PXRD data and then further confirmed by selected area electron diffraction (SAED).[42] A significant part of the solution was the realization that the building layers in the known ITQ-22 (FTC: **IWW**) with a 2D unit cell dimensions (b = 12.71 Å, c = 12.71 Å, and α = 90°) were identical to the building layers in the unknown ITQ-38 structure. The c-parameter of ITQ-38 is half of the a-parameter of ITQ-22, and thus, the structural model of ITQ-38 could be built based on the known ITQ-22 structure and then was further confirmed by high resolution transmission electron microscopy (HRTEM) images along the [101] direction. Figure 10 compares the ITQ-38 (**ITG**) and ITQ-22 (**IWW**) frameworks with the common building layer highlighted in gray. Large 12-rings are present in the layers of both structures. It is interesting to note that alternating distorted 6-rings and 10-rings are present in ITQ-38, while tilted 8-rings are present in ITQ-22. The structure determination of ITQ-3 (FTC: **ITE**) was also done by the same approach, based on the known RUB-13 structure (FTC: **RTH**).[32] The structural model of ITQ-3 was further confirmed by Rietveld refinement against synchrotron PXRD data.

DOI: 10.1021/acs.cgd.7b01410
Cryst. Growth Des. 2017, 17, 6821−6835

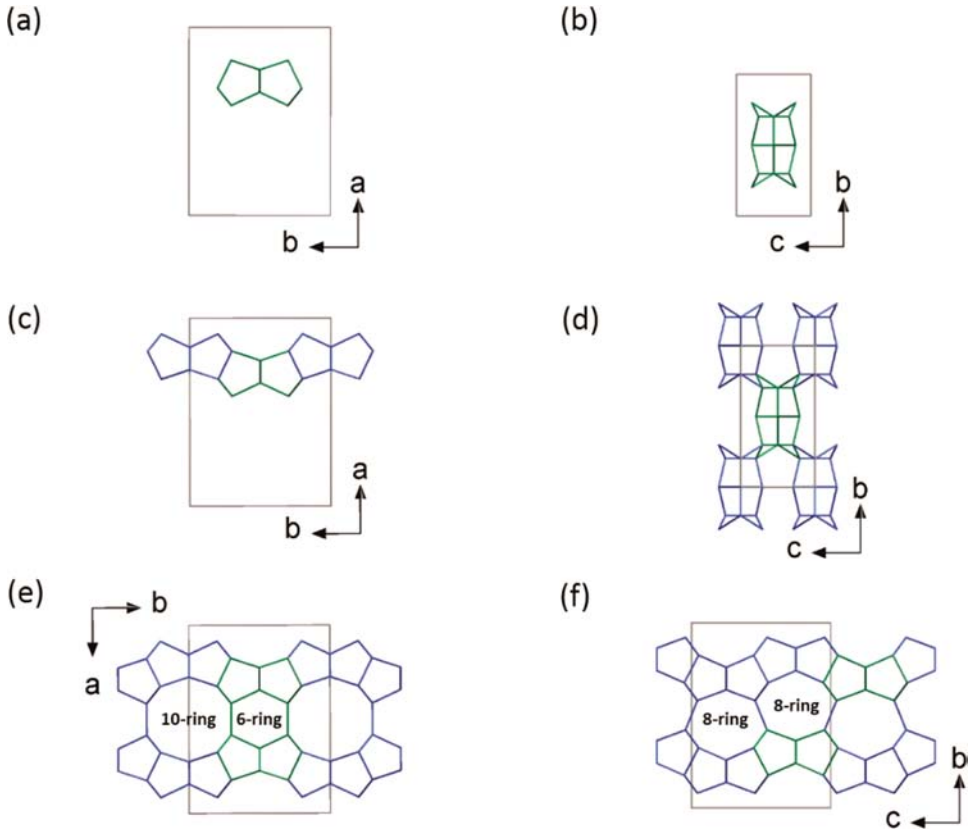

Figure 9. (a–e) Construction of the **FER** framework from the *fer* CBU. The *fer* CBU viewed along the [001] (a) and [100] (b) directions and the connectivity of adjacent *fer* CBUs viewed along [001] (c) and [100] (d). The **FER** framework viewed along [001] showing alternating 6-rings and 10-ring channels. (f) The **CDO** framework viewed along [100] showing 8-ring channels.

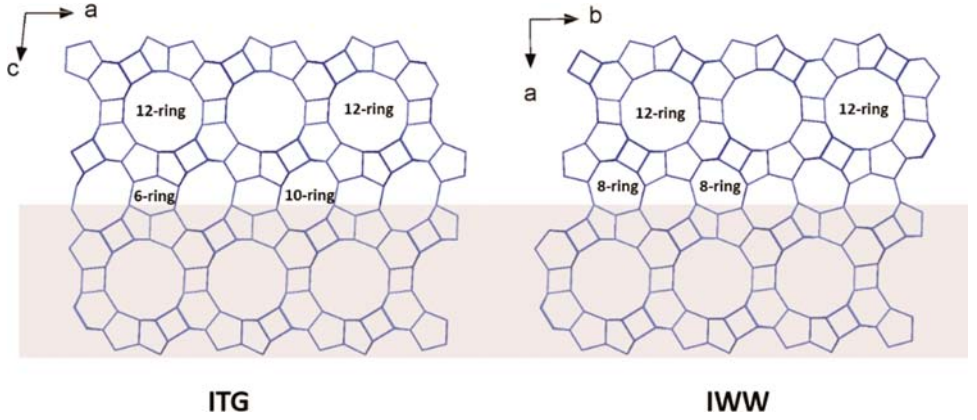

Figure 10. Comparison of framework projection of ITQ-38 (**ITG**) along [010] with that of ITQ-22 (**IWW**) along [001]. The common building layers are highlighted in gray.

ABC-6 Family. Most of the framework types in the ABC-6 family belong to the trigonal or hexagonal crystal systems. Table 8 lists the 22 framework types that belong to the ABC-6 family. They can be categorized into three subgroups according to the CBUs: only single 6-rings, only double 6-rings, and both single and double-6-rings, denoted group I, group II, and group III, respectively. The centers of the 6-rings are located at (0, 0), (2/3, 1/3), and (1/3, 2/3) in the *ab*-plane, respectively. Usually, the (0, 0) position is called A position as shown in Figure 11a. These adjacent planar 6-rings are further connected through tilted single 4-rings, forming a fully 4-connected framework (Figure 11b). The distinctive structural features of this family can be summarized as follows:

(1) The *a* (or *b*) parameters are within the range of 12.25–12.70 Å for group I, 13.65–13.75 Å for group II, and 12.85–13.20 Å for group III. This means the building units in the ABC-6 family can be estimated from the unit cell dimensions. Card observed this structural feature and Bennett et al. utilized it to solve the structure of AlPO-52 (FTC: **AFT**).[43] In 2013, Xie et al. also used this approach to solve the structure of a promising DeNO$_x$ catalyst SSZ-52 (FTC: **SFW**).[31] Both structures belong to the group II containing double 6-rings solely.

DOI: 10.1021/acs.cgd.7b01410
Cryst. Growth Des. 2017, 17, 6821–6835

Table 8. ABC-6 Family

	type material	FTC	space group	ring sizes	stacking sequence (repeating layer)	building units
Group I	Cancrinite	**CAN**	$P6_3/mmc$	12 6 4	AB(A)...(2)	single 6-rings only
	Sodalite	**SOD**	$Im\bar{3}m$	6 4	ABC(A)...(3)	12.25−12.70 Å
	Losod	**LOS**	$P6_3/mmc$	6 4	ABAC(A)...(4)	
	Liottite	**LIO**	$P\bar{6}m2$	6 4	ABACAC(A)...(6)	
	Afganite	**AFG**	$P6_3/mmc$	6 4	ABABACAC(A)...(8)	
	Franzinite	**FRA**	$P\bar{3}m1$	6 4	ABCABACABC(A)...(11)	
	Tounkite	**TOL**	$P\bar{3}m1$	6 4	CACACBCBCACB(C)...(12)	
	Marinellite	**MAR**	$P6_3/mmc$	6 4	ABCBCBACBCBC(A)...(12)	
	Farneseite	**FAR**	$P6_3/mmc$	6 4	ABCABABACBACAC(A)...(14)	
	Giuseppettite	**GIU**	$P6_3/mmc$	6 4	ABABABACBABABABC(A)...(16)	
Group II	Gmelinite	**GME**	$P6_3/mmc$	12 8 6 4	AABB(A)...(4)	double 6-rings only
	Chabazite	**CHA**	$R\bar{3}m$	8 6 4	AABBCC(A)...(6)	13.65−13.75 Å
	SAPO-56	**AFX**	$P6_3/mmc$	8 6 4	AABBCCBB(A)...(8)	
	AlPO-52	**AFT**	$P6_3/mmc$	8 6 4	AABBCCBBAACC(A)...(12)	
	SSZ-52	**SFW**	$R\bar{3}m$	8 6 4	AABBAABBCCBBCCAACC(A)...(18)	
Group III	Offretite	**OFF**	$P\bar{6}m2$	12 8 6 4	AAB(A)...(3)	double 6-rings and single 6-rings
	ZnAlPO-57	**AFV**	$P\bar{3}m1$	8 6 4	AABCC(A)...(5)	12.85−13.20 Å
	Erionite	**ERI**	$P6_3/mmc$	8 6 4	AABAAC(A)...(6)	
	TMA-EAB	**EAB**	$P6_3/mmc$	8 6 4	AABCCB(A)...(6)	
	ZnAlPO-59	**AVL**	$P\bar{3}m1$	8 6 4	ABBACCA(A)...(7)	
	Levyne	**LEV**	$R\bar{3}m$	8 6 4	AABCCABBC(A)...(9)	
	STA-2	**SAT**	$R\bar{3}m$	8 6 4	AABABBCBCCAC(A)...(12)	

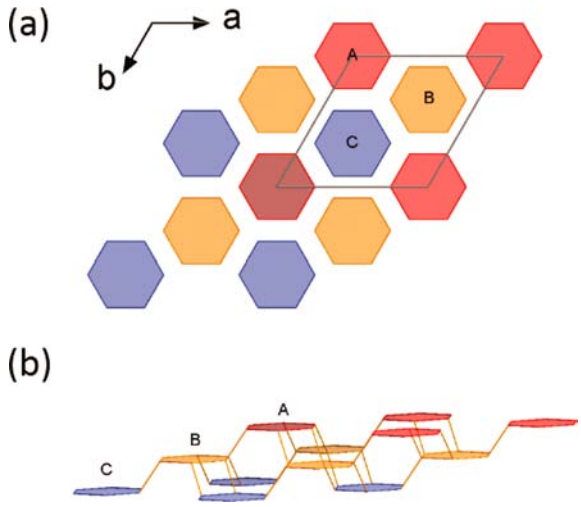

Figure 11. (a) Three different locations of the 6-rings in the unit cell, denoted A, B, and C. (b) Adjacent 6-rings connected by tilted 4-rings.

(2) The number of repeating layers (N) depends on the length of the c-axis of the hexagonal unit cell: $N = c/2.5$.
(3) Some members do not contain 6-rings at the C-location, giving rise to a 12-ring channel along the c-axis. Examples are the **CAN**, **OFF**, and **GME** framework types.
(4) As mentioned in the introduction, the phases of structure factors are crucially important for the structure determination. We also investigate the structural information in reciprocal space. The structure factor phases of some reflections within the ABC-6 family are fixed by symmetry constraints. Selecting **FAR**, **SFW**, and **SAT** frameworks from each subgroup as examples, the structure factor amplitudes and phases of $hk0$ reflections are calculated as shown in Figure 12. The phases of structure factors with indices 110, 220, 330, and 440 are constrained to be 180°, 180°, 0°, and 0°, respectively. The others (excluded the **SOD** framework due to the cubic unit cell setting) also follow this rule; see Figure S2 in Supporting Information. The constrained structure factor phases may be useful when determining unknown structures in the ABC-6 family. Furthermore, it may be possible to gain information about intrinsic structure factor phase relationships in other zeolite families.

Embedded Isoreticular RHO Family. The story of embedded isoreticular **RHO** family began with a very old zeolite ZSM-25, which was reported in 1981 by Mobil.[44] The researchers at POSTECH (Pohang, South Korea) had focused on this sample for a long time and done preliminary work about this material. For example, they utilized a variety of techniques, such as gas adsorption, IR, and Raman spectra, and identified that it is a small pore zeolite and has a large amount of 4-rings in the structure. However, the crystallographic information (unit cell, space group, and atomic coordinates) of ZSM-25 was still a mystery at that time.[38] We started investigating this material in 2013. Initially, ZSM-25 crystallized as nanocrystals, which is too small to be studied by SCXRD. It was not possible to obtain the unit cell of ZSM-25 from PXRD data. Thus, we used our RED technique to investigate this sample. Unfortunately, due to the severe beam damage, the resolution of the RED data was too low (2.5 Å) for a direct structure solution of ZSM-25 by direct methods. Luckily, the unit cell, possible space group, and the distribution of strong reflections can be obtained from the RED data. Three frameworks **KFI**, **RHO**, and **PAU** with the same Laue group ($m\bar{3}m$) as ZSM-25 were identified. It is important to note that the intensity distributions of strong reflections of **RHO**, **PAU**, and ZSM-25 in reciprocal space are similar. Figure 13a−b shows the similar distribution of strong reflections of **PAU** and ZSM-25, as highlighted in circles with the same colors. The structure factor phases of strong reflections from **PAU** were used to phase the corresponding strong reflections of the ZSM-25 structure. The structural model of ZSM-25 can be obtained by using the amplitudes from the experimental RED data of ZSM-25 and phases from **PAU** (Figure 13c).[29] We called this phasing

DOI: 10.1021/acs.cgd.7b01410
Cryst. Growth Des. 2017, 17, 6821−6835

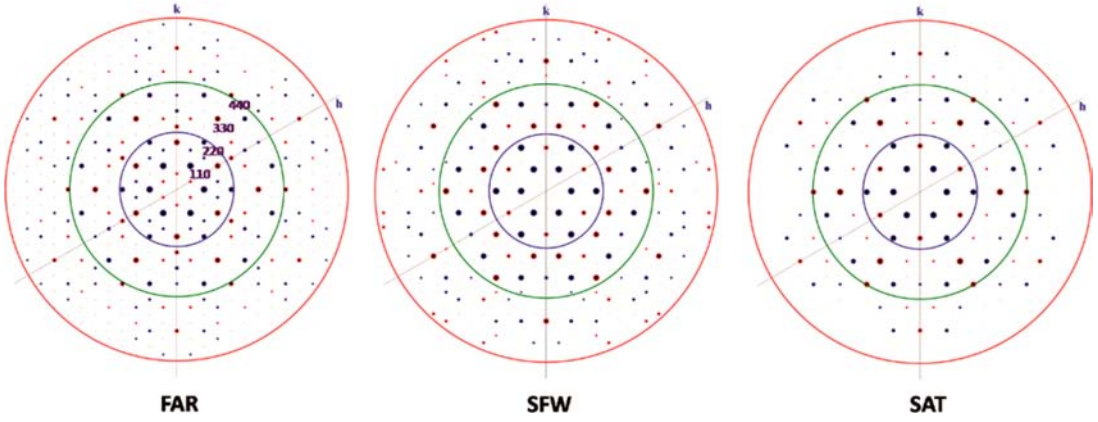

Figure 12. Comparison of structure factor amplitudes and phases of *hk*0 reflections calculated from **FAR**, **SFW**, and **SAT** frameworks. The red, green, and blue circles correspond to *d*-spacings of 1.0 Å, 1.6 Å, and 3.0 Å, respectively. The frameworks are idealized in the pure SiO_2 forms. Reflections in red and blue have phases of 0° and 180°, respectively. For clarity, the indices are given only for the **FAR** framework.

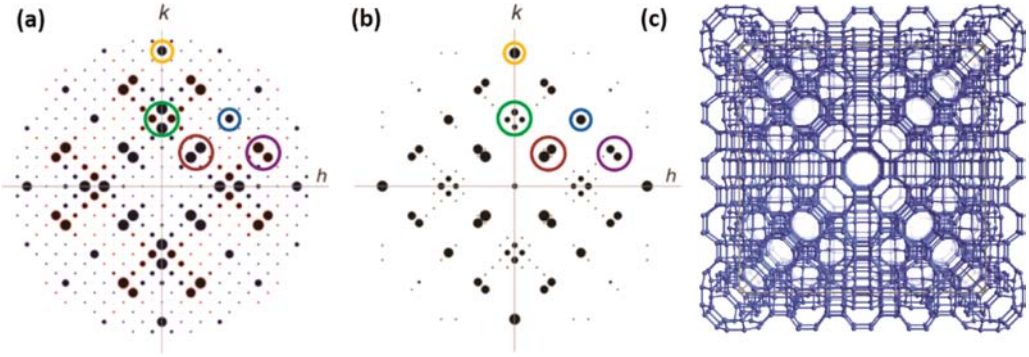

Figure 13. (a) Simulated diffraction pattern of the idealized **PAU** structure, with the structure factor phases marked in blue (180°) or red (0°). (b) The 2D slice of (*hk*0) cut from the 3D reciprocal lattice reconstructed from the RED data. The symmetry has been superimposed to allow for a better comparison. The similar distributions of strong reflections are marked by colored circles. (c) The framework structure of ZSM-25.

method the strong reflections approach. In 2015, IZA-SC approved this structure and then assigned FTC **MWF** for ZSM-25.

Both **PAU** and **MWF** frameworks are built from seven common cages as shown in Figure 14a. The **MWF** framework can be considered as an expanded version of **PAU**. The connection sequence between the *lta* cages in the **PAU** structure is *d8r-pau-d8r-pau-d8r*. Because of its intrinsic *I* centering, two interpenetrated scaffolds are generated as illustrated in Figure 14b. When a pair of *d8r* and *pau* cages (ca. 10 Å in length) is inserted in the unit cell edge of the **PAU** framework, the interpenetrated scaffolds of the **MWF** framework are constructed; see Figure 14c. The empty space between the scaffolds is filled by other four types of cages (*t-plg*, *t-oto*, *t-gsm*, and *t-phi* cages) as shown in Figure 14d–e.

It is interesting to note that hypothetical structures can be generated by continuing deleting or adding a pair of *d8r* and *pau* cages. For example, if a pair or two pairs of *d8r* and *pau* cages are removed from the unit cell edge of the **PAU** structure, a hypothetical structure ($\boldsymbol{a}$ = 25 Å and space group $Im\bar{3}m$) and the known **RHO** framework (type material: Rho) can be constructed, respectively. Thus, we denoted this series of zeolite structures as the **RHO** family. The Rho structure, the hypothetical structure (cubic unit cell a = 25 Å), the paulingite, and ZSM-25 structure are denoted as **RHO-G1** (first generation), **RHO-G2**, **RHO-G3**, and **RHO-G4**, respectively. Since the structure of **RHO-G2** is relatively simple, it can be built manually. However, the higher generations in the **RHO** family are challenging to build by hand. Therefore, we used the strong reflections approach again to generate a series of hypothetical structures **RHO-G5-G8**. The procedure is quite similar to the structure determination of ZSM-25 (phasing the strong reflections in the higher generation by using the structure factor phases from a lower generation). Furthermore, we take a further step that even the amplitudes of strong reflections are adopted from the lower generation, without using any experimental data. A series of energetically feasible zeolites as shown in Figure 15 had been predicted by this method. Finally Hong's group in POSTECH succeeded in synthesizing these predicted hypothetical structures.[29,45] The expansion of the 2-fold scaffolds in the **RHO** family resembles that in the metal–organic frameworks (isoreticular MOFs),[46−48] while the empty space between the scaffolds is filled by embedding four different cages. Thus, we called the members in the **RHO** family "embedded isoreticular" zeolite structures.

Conventionally, the related zeolite structures are compared by using common SBUs or CUBs in real space, such as the aforementioned **FER** and **CDO** frameworks. Here we propose an alternative way of identifying the structural relationships by exploring the intensity distribution of reflections (the structural coding) in reciprocal space. The strong reflections approach not only is a method for phasing but also links the structure prediction with the target synthesis. We list the following four unique merits of this approach below:

DOI: 10.1021/acs.cgd.7b01410
Cryst. Growth Des. 2017, 17, 6821−6835

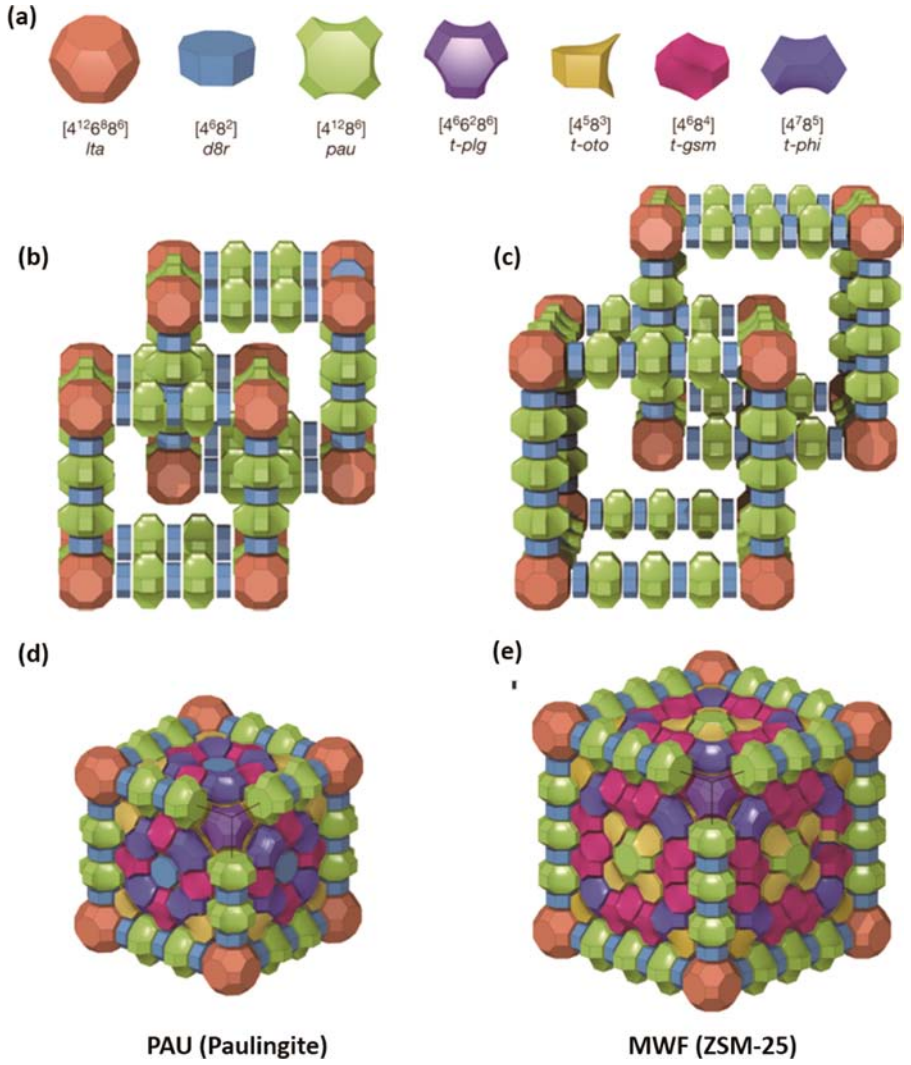

Figure 14. (a) The seven different cages: *lta*, *d8r*, *pau*, *t-plg*, *t-oto*, *t-gsm*, and *t-phi* found in **PAU** and **MWF** frameworks. (b–c) The connectivity of the *lta*, *d8r*, and *pau* cages in **PAU** and **MWF** frameworks. (d–e) The 3D frameworks of **PAU** and **MWF** with *t-plg*, *t-oto*, *t-gsm*, and *t-phi* cages embedded in the scaffolds.

(1) Identify a certain zeolite family. The similar intensity distribution of reflections is the crucial evidence of that. At the beginning, it is also challenging to identify the first two potential candidates. In the **RHO** family, the Laue group symmetry was used to search for the candidates among the existing frameworks. Inspired by our work, this database is expected to include simulated 3D electron or X-ray diffraction of each structure so that it will facilitate the identification of more related zeolite families.

(2) Solve unknown structures within a certain family. After the identification of the zeolite family, the structure factor phases of strong reflections, borrowed from the higher or lower generation, can be used for structure determination of the unknown one within this family. In this work, the phases of strong reflections in the **PAU** structure are utilized for unravelling the complexity of the ZSM-25 structure.

(3) Predict the energetically feasible hypothetical structures. Before this work, there have been a huge amount of hypothetical structures predicted. But few of them can be synthesized in the chemical lab. The hypothetical structures through the strong reflections approach are based on the known structures. The members in the family possess the same structural coding, which manifests in reciprocal space clearly as shown in Figure S3.

(4) Guide the target synthesis. It is of significance to note that the higher generations (from **G3** to **G8**) in the **RHO** family are synthesized by using the same organic structure directing agent tetraethylammonium (TEA). It has provided important synthetic information for the target synthesis of energetically feasible hypothetical structures.

CONCLUSIONS

In this article, we have explored the common structural features of the known zeolite structures in the database through real space and reciprocal space. In real space, the characteristic unit cell dimensions (such as 5 Å, 7.5 Å, 8.5 Å, 10 Å, and 12.7 Å), butterfly layers, and zeolites sharing the same building layers are illustrated and summarized. Through reciprocal space, the ABC-6 family and embedded isoreticular **RHO** family are investigated, by comparing the restricted structure factor phases

DOI: 10.1021/acs.cgd.7b01410
Cryst. Growth Des. 2017, 17, 6821–6835

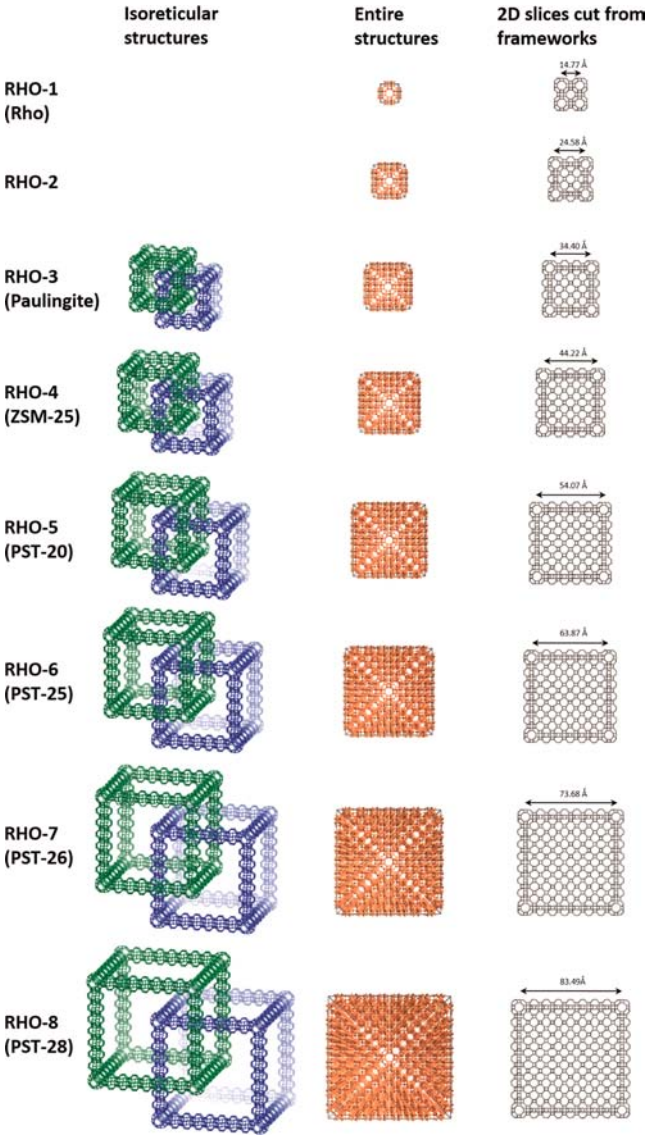

Figure 15. Expansion of isoreticular structures, entire structures, and 2D slices cut from the 3D frameworks in the **RHO** family.

and the intensity distribution of reflections, respectively. The results of the database mining provide new insights into the structural features of the existing zeolites, facilitate the prediction of more energetically feasibly zeolite families, and provide insightful synthetic information for the discovery of new zeolite structures.

■ ASSOCIATED CONTENT

Supporting Information

The Supporting Information is available free of charge on the ACS Publications website at DOI: 10.1021/acs.cgd.7b01410.

Double crankshaft chains in the ***STO** and **DON** frameworks; simulated electron diffraction patterns of the members in the ABC-6 family; simulated electron diffraction patterns of **RHO-G1-G8** structures in the **RHO** family (PDF)

■ AUTHOR INFORMATION

Corresponding Authors

*E-mail: pguo@dicp.ac.cn (P.G.).

*E-mail: xzou@mmk.su.se (X.Z.).

ORCID

Peng Guo: 0000-0001-5392-3915

Lei Wang: 0000-0002-4520-0685

Xiaodong Zou: 0000-0001-6748-6656

Funding

Swedish Research Council (VR), Swedish Governmental Agency for Innovation Systems (VINNOVA), Knut and Alice Wallenberg Foundation through the Project Grant 3DEM-NAT, and CAS Pioneer Hundred Talents Program (Y706071202).

Notes

The authors declare no competing financial interest.

■ ACKNOWLEDGMENTS

We thank Dr. Lynne McCusker and Dr. Christian Baerlocher for their help on the update in searching unit cells of idealized frameworks. We acknowledge financial support from the Swedish Research Council (VR), the Swedish Governmental Agency for Innovation Systems (VINNOVA), and the Knut and Alice Wallenberg Foundation through the project grant 3DEM-NAT, and CAS Pioneer Hundred Talents Program (Y706071202).

■ ABBREVIATIONS

SBU, secondary building unit; CBU, composite building unit; SCXRD, single crystal X-ray diffraction; PXRD, powder X-ray diffraction; RED, rotation electron diffraction; T, tetrahedra; 1D, one-dimensional; 2D, two-dimensional; 3D, three-dimensional; *d4r*, double 4-rings; *d6r*, double 6-rings; IZA-SC, International Zeolite Association-Structure Commission; FTC, framework type code; *nsc*, narsarsukite chains; *dnc*, double narsarsukite chain; *dcc*, double crankshaft chain; SAED, selected area electron diffraction; HRTEM, high resolution transmission electron microscopy; MOF, metal−organic framework; TEA, tetraethylammonium

■ REFERENCES

(1) Sun, J.; Bonneau, C.; Cantín, Á.; Corma, A.; Díaz-Cabañas, M. J.; Moliner, M.; Zhang, D.; Li, M.; Zou, X. *Nature* **2009**, *458*, 1154−1157.

(2) Jiang, J.; Jorda, J. L.; Yu, J.; Baumes, L. A.; Mugnaioli, E.; Diaz-Cabanas, M. J.; Kolb, U.; Corma, A. *Science* **2011**, *333*, 1131−1134.

(3) Meier, W. M.; Olson, D. H. In *Molecular Sieve Zeolites-I; Advances in Chemistry*; American Chemical Society, 1974; Vol. *101*, pp 155−170.

(4) Argauer, R. J.; Landolt, G. R. Crystalline Zeolite Zsm-5 and Method of Preparing the Same, US3702886A.

(5) Database of Zeolite Structures http://www.iza-structure.org/databases/.

(6) Meier, W. M.; Olson, D. H.; Baerlocher, Ch. *Atlas of Zeolite Framework Types*, 4th revised ed.; Elsevier: London, 1996.

(7) Treacy, M. M. J.; Higgins, J. B. *Collection of Simulated XRD Powder Diffraction Patterns for Zeolites*, 3rd revised ed.; Elsevier: London, 1996.

(8) The Nobel Prize in Chemistry, 1985 http://www.nobelprize.org/nobel_prizes/chemistry/laureates/1985/.

(9) Patterson, A. L. *Phys. Rev.* **1934**, *46*, 372−376.

(10) Christensen, J.; Oleynikov, P.; Hovmöller, S.; Zou, X. D. *Ferroelectrics* **2004**, *305*, 273−277.

(11) Oszlányi, G.; Sütő, A. *Acta Crystallogr., Sect. A: Found. Crystallogr.* **2008**, *64*, 123−134.

(12) Oszlányi, G.; Sütő, A. *Acta Crystallogr., Sect. A: Found. Crystallogr.* **2004**, *60*, 134−141.

DOI: 10.1021/acs.cgd.7b01410
Cryst. Growth Des. 2017, 17, 6821−6835

(13) Oszlányi, G.; Sütő, A. *Acta Crystallogr., Sect. A: Found. Crystallogr.* **2005**, *61*, 147−152.
(14) Wu, J.; Leinenweber, K.; Spence, J. C. H.; O'Keeffe, M. *Nat. Mater.* **2006**, *5*, 647−652.
(15) Baerlocher, C.; McCusker, L. B.; Palatinus, L. *Z. Kristallogr.* **2009**, *222*, 47−53.
(16) Baerlocher, C.; Gramm, F.; Massüger, L.; McCusker, L. B.; He, Z.; Hovmöller, S.; Zou, X. *Science* **2007**, *315*, 1113−1116.
(17) Zhang, D.; Oleynikov, P.; Hovmöller, S.; Zou, X. *Z. Kristallogr.* **2010**, *225*, 94−102.
(18) Wan, W.; Sun, J.; Su, J.; Hovmöller, S.; Zou, X. *J. Appl. Crystallogr.* **2013**, *46*, 1863−1873.
(19) Martínez-Franco, R.; Moliner, M.; Yun, Y.; Sun, J.; Wan, W.; Zou, X.; Corma, A. *Proc. Natl. Acad. Sci. U. S. A.* **2013**, *110*, 3749−3754.
(20) Smeets, S.; McCusker, L. B.; Baerlocher, C.; Xie, D.; Chen, C.-Y.; Zones, S. I. *J. Am. Chem. Soc.* **2015**, *137*, 2015−2020.
(21) Smeets, S.; Xie, D.; McCusker, L. B.; Baerlocher, C.; Zones, S. I.; Thompson, J. A.; Lacheen, H. S.; Huang, H.-M. *Chem. Mater.* **2014**, *26*, 3909−3913.
(22) Guo, P.; Strohmaier, K.; Vroman, H.; Afeworki, M.; Ravikovitch, P. I.; Paur, C. S.; Sun, J.; Burton, A.; Zou, X. *Inorg. Chem. Front.* **2016**, *3*, 1444−1448.
(23) Willhammar, T.; Burton, A. W.; Yun, Y.; Sun, J.; Afeworki, M.; Strohmaier, K. G.; Vroman, H.; Zou, X. *J. Am. Chem. Soc.* **2014**, *136*, 13570−13573.
(24) Hua, W.; Chen, H.; Yu, Z.-B.; Zou, X.; Lin, J.; Sun, J. *Angew. Chem., Int. Ed.* **2014**, *53*, 5868−5871.
(25) Jiang, J.; Yun, Y.; Zou, X.; Jorda, J. L.; Corma, A. *Chem. Sci.* **2015**, *6*, 480−485.
(26) Yun, Y.; Hernández, M.; Wan, W.; Zou, X.; Jordá, J. L.; Cantín, A.; Rey, F.; Corma, A. *Chem. Commun.* **2015**, *51*, 7602−7605.
(27) Schmidt, J. E.; Xie, D.; Rea, T.; Davis, M. E. *Chem. Sci.* **2015**, *6*, 1728−1734.
(28) Lorgouilloux, Y.; Dodin, M.; Mugnaioli, E.; Marichal, C.; Caullet, P.; Bats, N.; Kolb, U.; Paillaud, J.-L. *RSC Adv.* **2014**, *4*, 19440−19449.
(29) Guo, P.; Shin, J.; Greenaway, A. G.; Min, J. G.; Su, J.; Choi, H. J.; Liu, L.; Cox, P. A.; Hong, S. B.; Wright, P. A.; Zou, X. *Nature* **2015**, *524*, 74−78.
(30) Smeets, S.; Xie, D.; Baerlocher, C.; McCusker, L. B.; Wan, W.; Zou, X.; Zones, S. I. *Angew. Chem., Int. Ed.* **2014**, *53*, 10398−10402.
(31) Xie, D.; McCusker, L. B.; Baerlocher, C.; Zones, S. I.; Wan, W.; Zou, X. *J. Am. Chem. Soc.* **2013**, *135*, 10519−10524.
(32) Camblor, M. A.; Corma, A.; Lightfoot, P.; Villaescusa, L. A.; Wright, P. A. *Angew. Chem., Int. Ed. Engl.* **1997**, *36*, 2659−2661.
(33) Taylor, W. H. *Z. Kristallogr. - Cryst. Mater.* **1930**, *74*, 1−19.
(34) Taylor, W. H.; Jackson, R. *Z. Kristallogr. - Cryst. Mater.* **1933**, *86*, 53−64.
(35) Taylor, W. H.; Meek, C. A.; Jackson, W. W. *Z. Kristallogr. - Cryst. Mater.* **1933**, *84*, 373−398.
(36) Pauling, L. *Proc. Natl. Acad. Sci. U. S. A.* **1930**, *16*, 453−459.
(37) Pauling, L. *Z. Kristallogr. - Cryst. Mater.* **1930**, *74*, 213−225.
(38) Hong, S. B.; Paik, W. C.; Lee, W. M.; Kwon, S. P.; Shin, C.-H.; Nam, I.-S.; Ha, B.-H. *Stud. Surf. Sci. Catal.* **2001**, *135*, 186.
(39) Elomari, S.; Burton, A. W.; Ong, K.; Pradhan, A. R.; Chan, I. Y. *Chem. Mater.* **2007**, *19*, 5485−5492.
(40) Dodin, M.; Paillaud, J.-L.; Lorgouilloux, Y.; Caullet, P.; Elkaïm, E.; Bats, N. *J. Am. Chem. Soc.* **2010**, *132*, 10221−10223.
(41) Guo, P.; Wan, W.; McCusker, L.; Baerlocher, C.; Zou, X. *Z. Kristallogr. - Cryst. Mater.* **2015**, *230*, 301−309.
(42) Moliner, M.; Willhammar, T.; Wan, W.; González, J.; Rey, F.; Jorda, J. L.; Zou, X.; Corma, A. *J. Am. Chem. Soc.* **2012**, *134*, 6473−6478.
(43) Bennett, J. M.; Kirchner, R. M.; Wilson, S. T. *Stud. Surf. Sci. Catal.* **1989**, *49*, 731−739.
(44) Doherty, H. G.; Plank, C. J.; Rosinski, E. J. Crystalline zeolite ZSM-25. US4247416A, January 27, 1981.
(45) Shin, J.; Xu, H.; Seo, S.; Guo, P.; Min, J. G.; Cho, J.; Wright, P. A.; Zou, X.; Hong, S. B. *Angew. Chem., Int. Ed.* **2016**, *55*, 4928−4932.
(46) Yaghi, O. M.; O'Keeffe, M.; Ockwig, N. W.; Chae, H. K.; Eddaoudi, M.; Kim, J. *Nature* **2003**, *423*, 705−714.
(47) Deng, H.; Grunder, S.; Cordova, K. E.; Valente, C.; Furukawa, H.; Hmadeh, M.; Gándara, F.; Whalley, A. C.; Liu, Z.; Asahina, S.; Kazumori, H.; O'Keeffe, M.; Terasaki, O.; Stoddart, J. F.; Yaghi, O. M. *Science* **2012**, *336*, 1018−1023.
(48) Eddaoudi, M.; Kim, J.; Rosi, N.; Vodak, D.; Wachter, J.; O'Keeffe, M.; Yaghi, O. M. *Science* **2002**, *295*, 469−472.

DOI: 10.1021/acs.cgd.7b01410
Cryst. Growth Des. 2017, 17, 6821−6835